Light Metals 2011 *Edited by: Stephen J. Lindsay*
TMS (The Minerals, Metals & Materials Society), 2011

BUBBLE TRANSPORT BY ELECTRO-MAGNETOPHORETIC FORCES AT ANODE BOTTOM OF ALUMINIUM CELLS

Valdis Bojarevics and Alan Roy

University of Greenwich, School of Computing and Mathematical Sciences,
30 Park Row, London, SE10 9LS, UK
V.Bojarevics@gre.ac.uk

Abstract

Electrically conducting and nonconducting particles and bubbles experience additional forcing in a liquid which carries electric current. These so called electro-magnetophoretic forces are well known in metallurgical applications, like metal purification in vacuum-arc remelting, electro-slag processes, impurity removal or concentration change in special castings. However, the effect of electro-magnetophoretic forces has never been considered for aluminium cells where the gas bubbles evolving in the liquid electrolyte are surrounded by an electric current and significant magnetic fields. We present models to estimate the effect of electric current flow in the vicinity of the bubbles and the additional pressure distribution resulting from the magnetic forces in the surrounding liquid electrolyte. According to the estimates, this force becomes important for bubbles exceeding 2 mm in size, and could be sufficient to overcome the typical drag force associated with electrolyte flow thereby opposing motion of the bubble along the base of the anode when it is inclined at a slight angle. The effect could explain certain features of the anode effect onset. Mathematical models and numerical results are presented and a further implementation in the general MHD code for the aluminium cell design is discussed.

Introduction

The presence of gas bubbles is an inherent feature of the electrolytic aluminium production cells. Typically CO_2 gas bubbles are produced at a rate proportional to the electric current magnitude yielding approximately 2.5 m^3 of gas per kg of aluminium produced. A detailed description of the bubble creation, detachment and transport is given in many publications ([1-5] are recent examples). The detached bubbles during the aluminium reduction are typically of 3-5 mm in size [1] and can grow due to collision and coalescence. On extreme occasions their volume can reach 100 ml. The presence of bubbles contributes significantly to the overall voltage loss of an individual cell (about 0.25 V from the total of 4 - 4.5 V) [2]. The usual assumption is that the bubbles are transported due to the buoyancy driven flow originating from the bubble escape into the side channels at the edges of the anodes [3-5]. The shape of the anode bottom is recognized as an important factor to facilitate the initial buoyancy force moving the bubbles [3]. In addition to this the electromagnetically driven flow exerts an additional drag force which contributes to the bubble transport along the flow streamlines, and could change the drag coefficient due to local nonuniformity of the electrical current around the bubble [9].

However a less recognized but significant contribution to the force balance on a moving bubble arises from the so called electro-magnetophoretic forces which were first theoretically analyzed by Leenov and Kolin in 1954 [6]. They derived expressions for electrically conducting and nonconducting particles (or bubbles) in the presence of an electric current and magnetic field in the surrounding liquid. They suggested possible applications like separation of particles and opposing the gravity effects. Since then metallurgists were keenly exploiting the electro-magnetophoretic force for a variety of applications, such as removal of inclusions from steel melt [7], concentrating the insulating bubbles and inclusions [8], and for many other purposes [9]. It is important to note that not only the electrically conducting particles experience the effect of the electromagnetic force due to the current passing through them and interacting with the overall magnetic field. The electrically nonconducting particles in an electric current carrying fluid will experience significant force due to the pressure distribution gradient arising with the electromagnetic force action in the surrounding fluid. The physical effect is very similar to the buoyancy force created by the vertical pressure stratification in the fluid in the presence of gravity. With the electromagnetic force the pressure gradient can be created in any direction in the fluid carrying electric current.

In this paper we attempt to derive a very simple mathematical model for a bubble of hemispherical shape attached at the bottom of the anode in an aluminium electrolysis cell. The mathematical expression for the electro-magnetophoretic force is used to estimate a possible effect on the bubble transport and compared to the viscous drag force from the integral large scale bubble driven and electromagnetically driven flow . By comparing the buoyancy force at the bottom of a sloped anode with the electro-magnetoforetic force it is possible to find conditions when a bubble of larger size could be trapped in a stationary position for some time. This observation can yield further insight to the anode effect mechanisms and the conditions triggering the onset of the anode effect [10].

The inclusion of the electro-magnetophoretic effect with the bubble distribution models is a possible development for the wave model and the dynamic interaction with the electromagnetic field as implemented in the MHD numerical code [11].

The setup for a mathematical model

Before considering the local bubble model it is important to have a view to an integral picture of the whole aluminium cell. For this purpose we will use the results obtained from our previous coupled MHD models for the whole cell [11]. The interface between the liquid metal and electrolyte forms a nearly stationary dome like shape, as shown in Figure 1 for the case of a 500 kA cell. The interface shape can be variable if the cell is close to the stability limit when the waves start appearing. For a stable cell the time average deformation of the aluminium-bath interface causes redistribution of the electric current, which accelerates consumption of the anode bottom in areas where the anode-cathode distance (ACD) is reduced. The time average shape of the anode block above the metal interface shown in Figure 1 will eventually assume a shape similar to that computed in Figure 2. Note that the bottom shape is shown with an exaggerated scaling in the z-axis direction (about 15 times).

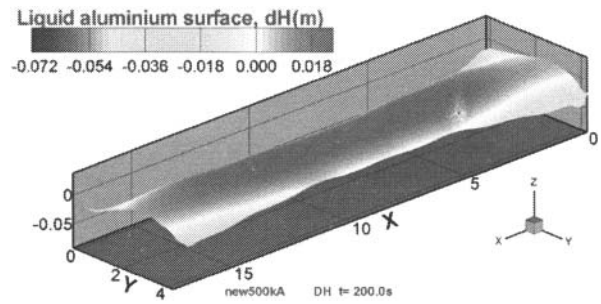

Figure 1. The interface shape of a 500 kA cell.

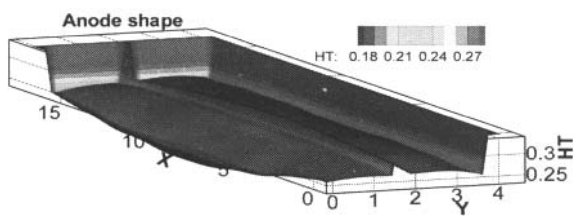

Figure 2. The view to the bottom of all anode blocks (without divisions between individual anodes) as computed for the electric current adjustment to the constant ACD condition.

The electric current distribution in the electrolyte layer below the anodes is approximately uniform at the density 0.7 A/cm^2. The magnetic field computed for the 500 kA cell is shown in Figure 3. From the direction of the arrows and the colour flooding of the contours it is evident that the B_x component (along the long side of the cell) is the dominant contribution to the total magnetic field. This could be generalized for various other cells we have considered modelling. The B_x field is unavoidably present, it is the dominant component, and it can not be affected significantly by rearranging the cell bus bar network supplying the electric current. The B_x field is mainly produced by the vertical current in the whole cell and the horizontal currents in the liquid metal and the cathode collector bars. Typically the B_x field has a nearly linear gradient in the y-axis direction, increasing in magnitude away from the cell central axis.

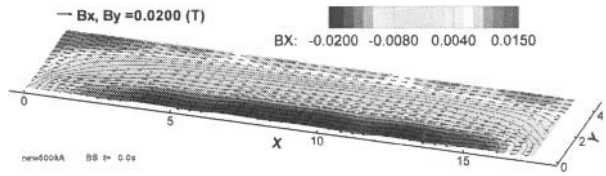

Figure 3. The computed magnetic field in the electrolyte layer for the 500 kA cell.

A simple model for a hemi-spherical bubble

In order to obtain a quantitative description of the electro-magnetophoretic force acting on a gas bubble attached or slowly moving along the anode bottom, let us consider an idealized situation shown in the Figure 4. A hemispherical shape bubble is positioned somewhere in the middle of a mildly sloped carbon anode, from which the electric current flows uniformly downwards. The actual current distribution is obtained using the commercial 3d electromagnetics module in the package COMSOL.

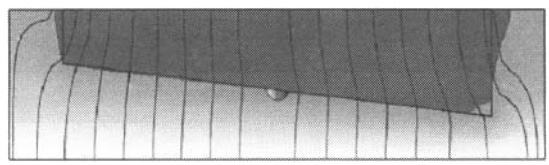

Figure 4. The hemi-spherical bubble at the bottom of carbon anode with the computed electric current lines.

For the analytical derivation we can use the problem setup shown in the Figure 5. The electric current $\mathbf{J} = -J_{0z}\,\mathbf{e_z}$ has only the vertical component of constant value J_{0z}. The magnetic field is assumed to have only the B_x component given as $\mathbf{B} = B_{0x}\,y/L_y\,\mathbf{e_x}$, where B_{0x} is the magnitude of the field at the external edge of the anode whose width is L_y. The Lorentz force acting in the fluid (electrolyte) has only a single y-directed component given by

$$F_y = -\frac{B_{0x}\,y\,J_{0z}}{L_y}\,. \qquad (1)$$

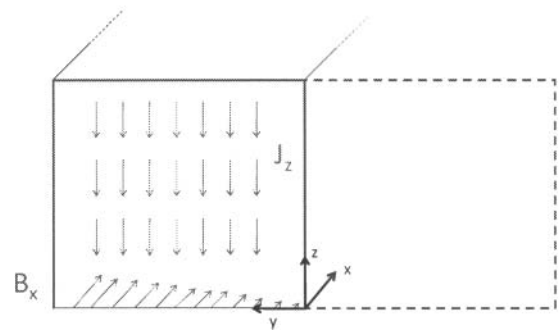

Figure 5. Setup for the analytical model with the uniform electric current J_z and linearly growing magnetic field B_x.

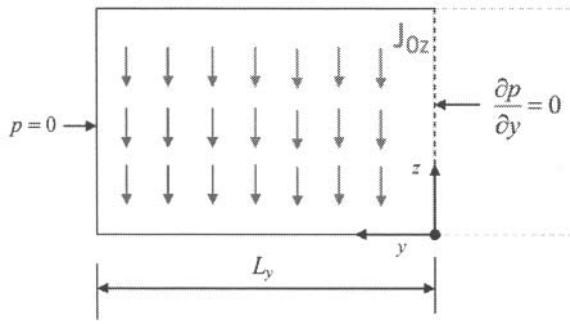

Figure 6. The model for obtaining the pressure $p(y)$ - created by the uniform electric current Jz and linearly growing magnetic field Bx.

The electromagnetic force (1) acting in the fluid will create a pressure $p(y)$ distribution according to the boundary conditions chosen to represent the situation under the anodes. Figure 6 is representative of one half of the cell with the symmetry axis at y = 0, where the appropriate symmetry condition of zero normal derivative is imposed. At the left edge of the electrode we assume a constant hydrostatic pressure under the given depth of the electrolyte. Since mathematically the pressure is defined to the accuracy of an arbitrary constant, we can choose $p(y=L_y)=0$. To find the pressure distribution we need to solve the hydrostatic equation

$$\nabla\cdot(\nabla p)=\nabla\cdot(\boldsymbol{J}\times\boldsymbol{B}), \tag{2}$$

which implies that

$$\frac{\partial^2 p}{\partial y^2}=\frac{\partial}{\partial y}F_y=-\frac{B_{0x}J_{0z}}{L_y}\ . \tag{3}$$

The solution of (3) with the given boundary conditions is

$$p=-\frac{B_{0x}J_{0z}}{2L_y}y^2+\frac{1}{2}B_{0x}J_{0z}L_y. \tag{4}$$

Suppose that the centre of the bubble is at y = y_b . The total force acting on the bubble from the fluid is the surface integral over the hemi-spherical surface:

$$\mathbf{F_p}=-\iint p d\mathbf{S_R}, \tag{5}$$

where the minus sign appears because the normal vector to the fluid facing the bubble is opposite to the $\mathbf{e_R}$ direction in a spherical co-ordinate system with the origin at the bubble centre. To compute the integral (5) we first shift the origin to the bubble centre by transformation $y'=y-y_b$:

$$p=-\frac{B_{0x}J_{0z}}{2L_y}(y'+y_b)^2+\frac{1}{2}B_{0x}J_{0z}L_y. \tag{6}$$

Then by replacing $y'=r_b\sin\theta\sin\varphi$ in local spherical co-ordinates after the transformation, we can express the y-component of the force as:

$$\begin{aligned}\mathbf{F_p}\cdot\mathbf{e}_y&=-\iint p d\mathbf{S_R}\cdot\mathbf{e}_y=\\&=-\iint p r_b^2\sin^2\theta\sin\varphi d\theta d\varphi.\end{aligned} \tag{7}$$

The expression (6) for $p(y')$ contains even and odd terms in powers of $y'=r\sin\theta\sin\varphi$, of which only the odd powers (linear in this case) will contribute to the total integral over the symmetrical bubble surface. This means that the total force in the y-direction is

$$\begin{aligned}F_{py}&=\frac{B_{0x}J_{0z}}{L_y}y_b\int_{\pi/2}^{\pi}\int_0^{2\pi}r_b^3\sin^3\theta\sin^2\varphi d\theta d\varphi=\\&=\frac{B_{0x}J_{0z}}{L_y}y_b\frac{2\pi r_b^3}{3}=B_{0x}J_{0z}\frac{y_b}{L_y}V_b,\end{aligned} \tag{8}$$

where V_b is the volume of the hemi-spherical bubble. It is easy to make more general conclusions, remarking that the expression (8) coincides with that derived by Leenov-Kolin in the case of uniform current and uniform field, in fact,

$$\mathbf{F_p}=-(\mathbf{J}\times\mathbf{B})_{fluid}\ V_b. \tag{9}$$

The expression (9) shows that there will be a force acting on a non-conducting bubble which is equal to that computed over the fluid volume in the absence of the bubble, but with the minus sign. Some authors [8] introduce form factors to represent different shapes of particles or bubbles compared to the spherical volume expression. The expression in (9), however, is more general.

Returning to the electrolysis cell situation, it is instructive to analyze the expression (8). We can see that the force increases linearly with the bubble distance y_b from the cell centre. The force grows as the third power of the size of the bubble. It will increase proportionally to the magnitudes of the current density Jz and the maximum magnetic field B_{0x}.

Let us estimate the relative values of the electro-magnetophoretic force and the drag force acting on a bubble in a large scale flow driven by either the total effect of bubbles escaping at anode edges (bubble driven flow) or the electromagnetic force-driven large scale horizontal flow. Suppose that, for simplicity, the bubble is of spherical shape. The drag force on a small spherical bubble is given by Stokes formula, modified for the slip boundary condition:

$$\mathbf{F}_d=-4\pi\eta r_b\mathbf{v}, \tag{10}$$

where η is fluid viscosity. When the electro-magnetophoretic force is equal in magnitude to the drag force, the bubble is trapped in the flow or deviates from the fluid flow line direction (if the forces are not aligned). The condition for a spherical bubble can be expressed by multiplying expression (8) by a factor of 2:

$$\mathbf{F}_d = \mathbf{F}_p,$$
$$4\pi\eta r_b |\mathbf{v}| = \frac{B_{0x} J_{0z}}{L_y} y_b \frac{4\pi r_b^3}{3}. \quad (11)$$

Assuming typical values for the electrolyte circulation velocity |v| equal to 0.1 m/s, fluid viscosity 0.002 kg/(s.m), the maximum magnetic field B_{0x} = 0.02 T, the electric current density J_{0z} = 7000 A/m^2, and the position of the bubble close to the edge $y_b = L_y$, the minimum possible size for a bubble, stopped by the action of the electro-magnetophoretic force opposing the drag from the flow, is

$$r_b = 2.07 \cdot 10^{-3} \ (m) \ \approx \ 2 \ mm. \quad (12)$$

This estimate is well within the range of typical bubble sizes (3 – 5 mm) after detachment in the electrolysis process [1]. For a 4 mm bubble the magnetic pressure force will be 4 times larger than the drag force under the assumed conditions, and the bubble will start moving against the incoming flow.

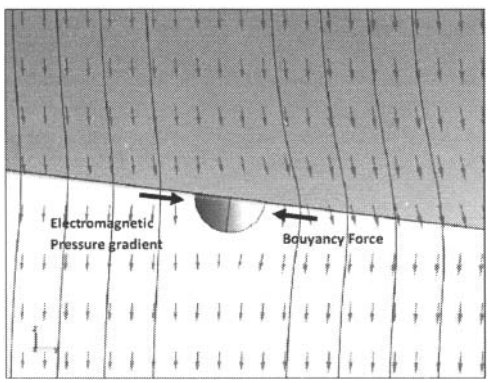

Figure 7. Schematic representation of a possible force balance for a bubble positioned at the bottom of a mildly sloped anode.

Figure 7 indicates another situation when the bubble at the bottom of a mildly sloped anode is trapped in a stationary position due to the balance of the buoyancy force F_g and the magnetic pressure force F_p:

$$\mathbf{F}_p = \mathbf{F}_g,$$
$$B_{0x} J_{0z} \cdot V_b \approx \rho_e g \sin\alpha \cdot V_b, \quad (13)$$

where $\rho_e g \sin\alpha$ is the effective buoyancy force driving the bubble upwards along a gently inclined slope of angle α to the horizontal. A simple calculation, using similar data as in the previous example (assuming an electrolyte density of 2100 kg/m^3) would suggest that when the anode bottom is sloped at about 0.45 degrees the bubble motion could be stopped. This is a very mild slope, but nevertheless quite realistic in operating conditions.

Numerical results for the local hydrodynamics

In this section we investigate the effect of the flow which could arise due to the pressure distribution obtained from the expression (4), which can affect the validity of the pressure distribution. The original derivation by Leenov-Kolin [6] assumed an infinite volume of fluid, and the authors proved analytically that the arising viscous flow due to the pressure distribution does not affect the resultant force. We have set up an idealized fluid dynamic model using COMSOL to investigate possible flow effects on the resulting pressure distribution. The fluid flow field shown in Fig. 8 was computed using the boundary conditions for pressure in Figure 6 and the previous distribution of electric current and magnetic field which yielded the force distribution (1) in the liquid electrolyte. This flow has no similarity to a real aluminium cell where multiple anodes are present and the flow results from the integral effect of all electromagnetic interactions. The purpose of this simple model is to compute possible variation in the pressure field with velocity present.

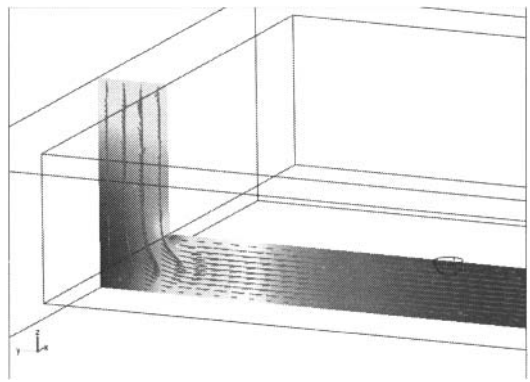

Figure 8. The computed pressure and the flow driven from the side channel along the anode bottom to the central channel of the cell.

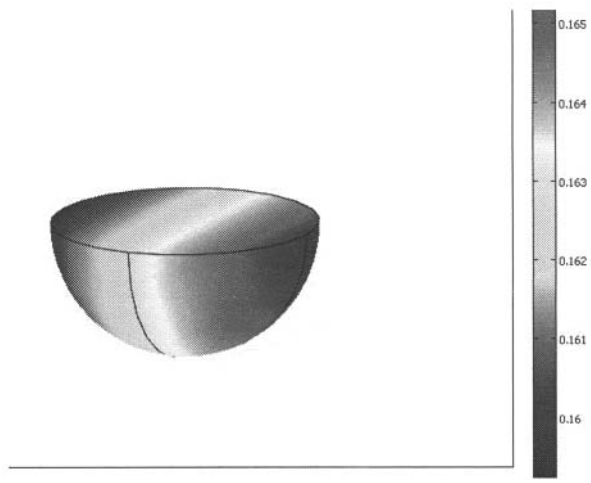

Figure 9. The computed pressure distribution on the surface of the hemi-spherical bubble when fluid flow is present..

Figure 8 demonstrates the pressure distribution in the whole bottom space, showing a similar pressure gradient to that obtained

analytically (4). Locally at the hemi-spherical bubble surface the computed pressure distribution is shown in the Figure 9.
Figure 10 presents the computed pressure as a function of position along a line in the electrolyte just below the bubble (solid blue line); the dotted black line represents a fitted quadratic function. The fitted quadratic function has the equation

$$p = -35.597y^2 + 14.752y + 0.1694, \qquad (14)$$

Encouragingly the pressure is well-described by a quadratic function. We may compare the coefficient of the quadratic term with the analytical expression derived earlier (4), substituting $B_{0x} = 0.02$ T:

$$p = -\left(\frac{0.01J_{0z}}{L_y}\right)y^2 + 0.01J_{0z}L_y. \qquad (15)$$

The 3D model has end effects associated with the flow which would explain why the fitted curve has a linear term in y which is not present in the analytical expression. Additionally, since only the gradient of pressure drives the flow there is a constant offset associated with the gauge. If we assume that the current density in the 3D model is $J_{0z} = 7 \cdot 10^3$ A/m^2, then the analytical coefficient of the quadratic term approximately matches the value in (14), which would suggest that the 3D simulation is producing numbers of the correct order of magnitude.

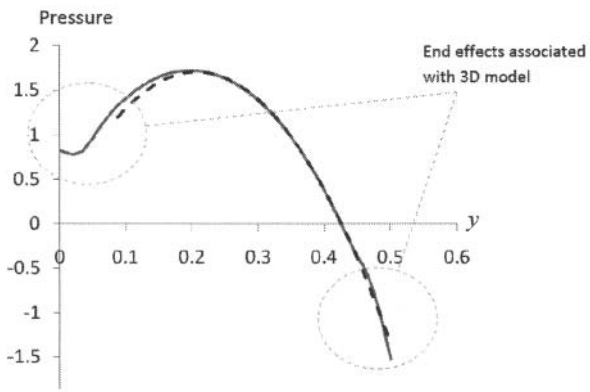

Figure 10. The computed pressure distribution at the mid-plane of the electrolyte passing through the position of the bubble as computed for the flow in Figure 8.

Numerical results for the electric current distribution

It is of certain interest to compare the electric current distribution on the anode when a bubble or cluster of bubbles are attached to the bottom of the anode. For this purpose we used the simple 3D model shown schematically in Figure 11.

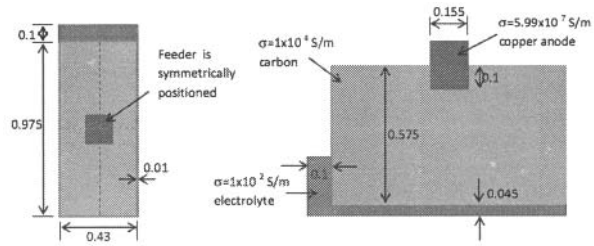

Figure 11. Schematic 3D geometry for the anode and the electrolyte.

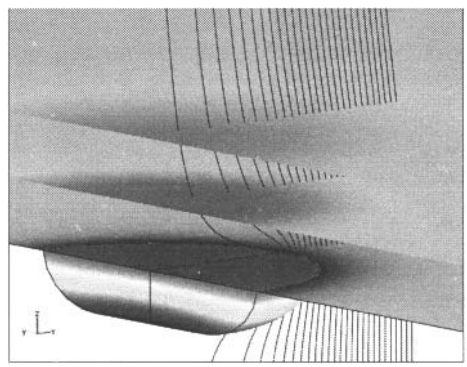

Figure 12. Streamlines of electric current around a large bubble (r=20 cm) attached at the bottom of the anode.

Initially the current was computed in the absence of any bubbles at the bottom. Fig. 13 (blue curve) shows the percentage of the total current exiting the anode on the side surfaces as a function of the ACD distance. Also shown in Fig. 13 are, for comparison, results for the case when a large bubble of radius 20 cm is present. The local distribution of electric streamlines around the bubble is shown in Figure 12. The results indicate that the presence of the bubble adjusts the effective ACD distance and makes the current path through the side faces of the anode more favorable. The nonlinear resistance due to the electrochemical voltage drop was not accounted for as this is not the subject of the present study.

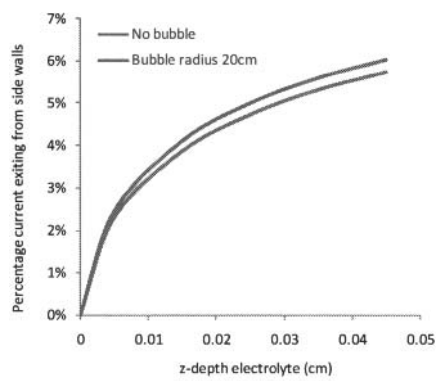

Figure 13. The computed ACD dependence of the electric current percentage exiting the side wall when the large bubble is present compared to the situation without the bubble.

Conclusions

Analysis of the electro-magnetophoretic forces acting on bubbles in the aluminium reduction cells suggests that their presence could significantly affect bubble transport, concentration and detachment. The models presented give numerical estimates of the effect of electric current flow in the vicinity of the bubbles including the additional pressure distribution resulting from the magnetic forces in the surrounding liquid electrolyte. According to these estimates, this force becomes important for bubbles exceeding 2 mm in size. The force is sufficient to overcome the typical drag force due to electrolyte flow, and could potentially prevent translational displacement of the bubble along the base of the anode when it is inclined at a gentle gradient. The effect could explain certain features of the anode effect onset. A further implementation in the general MHD code for the aluminium cell design is considered for future work.

References

1. K. Vekony and L. I. Kiss, "Morphology of Two-Phase Layers with Large Bubbles". Metallurgical and Materials Transactions, 41B, 1006-1017 (2010).

2. M.A. Cooksey, M.P. Taylor and J.J. Chen, "Resistance due to gas bubbles in aluminium reduction cells". Journal of Metals, Feb. (2008), 51-57.

3. Z. Zoric, T. Thonstad and T. Haarberg, "The influence of the initial shape and position of an anode and the curvature of the aluminium on the current distribution in prebaked aluminium cells". Metallurgical and Materials Transactions, 30B, 341-348 (1999).

4. Y. Feng, M.A. Cooksey and M.P. Schwarz, "CFD modelling of alumina mixing in aluminium reduction cells". *TMS Light Metals* (2010), 455-460.

5. D.S. Severo, V. Gusberti, "A modelling approach to estimate bath and metal heat transfer coefficients". *TMS Light Metals* (2009), 557-562.

6. D. Leenov and A. Kolin, "Theory of electromagnetophoresis". Journ. Chem. Phys., 22, N 4, 683-688 (1954).

7. T. Toh, H. Yamamura, H. Kondo, M. Wakoh, Sh. Shimasaki and S. Taniguchi, "Kinetics Evaluation of Inclusions Removal During Levitation Melting of Steel in Cold Crucible", ISIJ International, 47, No 11, 1625-1632 (2007).

8. J.W. Haverkort and T.W.J. Peeters, "Magnetohydrodynamic effects on insulating bubbles and inclusions in the continuous casting of steel", Metallurgical and Materials Transactions, Online First (2010).

9. V. Bojarevics, J. Freibergs, E. Shilova and E. Shcherbinin, Electrically Induced Vortical Flows, Kluwer Academic Publishers, Dordrecht, Boston, London, p 248 (1989).

10. J. Thonstad and H. Vogt, "Terminating anode effects by lowering and raising the anodes". *TMS Light Metals* (2010), 461-466.

11. V. Bojarevics and K. Pericleous, "Shallow Water Model for Aluminium Electrolysis Cells with Variable Top and Bottom". *In Proceedings of TMS Light Metals* (2008), 403-408.